Journal of Catalysis **189,** 117–128 (2000)
Article ID jcat.1999.2694, available online at http://www.idealibrary.com on IDEAL®

Co/Ni/Mg/Al Layered Double Hydroxides as Precursors of Catalysts for the Hydrogenation of Nitriles: Hydrogenation of Acetonitrile

Bernard Coq,[1] Didier Tichit, and Solange Ribet

Laboratoire de Matériaux Catalytiques et Catalyse en Chimie Organique, UMR 5618 CNRS/Ecole Nationale Supérieure de Chimie de Montpellier, 8, Rue Ecole Normale, 34296 Montpellier Cedex 5, France

Received June 4, 1999; revised September 3, 1999; accepted September 28, 1999

Layered double hydroxides (LDHs) with a hydrotalcite-like structure and containing $Ni^{2+}/Co^{2+}/Mg^{2+}/Al^{3+}$ cations in different amounts were prepared and activated in various conditions. Depending on the chemical composition and the calcination temperature, mixed-oxide and spinel-like phases of complex compositions are obtained. They lead to well-dispersed bimetallic phases of high metal loadings upon reduction. Temperature-programmed reduction by H_2 showed that the introduction of Mg decreases the reducibility of metals and that most of the Ni and Co are together in bimetallic aggregates. These catalysts were tested in the gas-phase hydrogenation of acetonitrile between 350 and 450 K and with a H_2/CH_3CN molar ratio of ca. 33. The main product is ethylamine (MEA); secondary products are *N*-ethyl,ethylimine at low conversion, diethylamine and triethylamine at high conversion. The Ni-free catalyst is three orders of magnitude less active than the Ni-containing samples. The by-products are formed by condensation between "imine-" and "amine-like" adsorbed species on metal and acid sites (bifunctional mechanism) and on the metal sites alone as well. The tuned addition of Mg ($Mg/(Mg + Ni + Co) \approx 0.25$) lowers the surface acidity and the bifunctionalized formation of by-products consequently. A net increase in MEA selectivity is further reached thanks to the formation of bimetallic NiCo phases. It is proposed that by-product formation on the metal surface occurs by condensation at Ni^0 sites between multibonded adsorbed species, which could be of the acimidoyl and aminomethylcarbene types. The first role of Co is the dilution of the Ni surface in small ensembles less prone to accomodate neighboring multibonded species. The IR spectroscopy of adsorbed CO provided evidences of the dilution of Ni by Co in bimetallic NiCo particles. A catalyst obtained from the Co/Ni/Mg/Al (0.27/0.26/0.22/0.25) LDH, calcined at 393 K and then reduced at 893 K, exhibits the highest selectivity to ethylamine, 98.2% at 10% CH_3CN conversion.

Key Words: **layered double hydroxides; hydrotalcite; Ni, Co bimetallic catalysts; hydrogenation; acetonitrile; nitrile; IR spectroscopy.**

INTRODUCTION

Layered double hydroxides (LDHs), or anionic clays or hydrotalcite-type compounds, of general formula $[M^{II}_{1-x}M^{III}_x(OH)_2]^{x+}[A^{m-}_{x/m}] \cdot nH_2O$ contain divalent (Mg^{2+}, Zn^{2+}, Ni^{2+}, Co^{2+}, Cu^{2+}, ...) and trivalent cations (Al^{3+}, Cr^{3+}, ...), the ratio M^{II}/M^{III} being between 1.5 and 4. These materials are promising precursors of multicomponent catalysts and applications in this field are described in recent reviews (1, 2). Upon calcination they afford simple oxides, mixed oxides of the $M^{II}(M^{III})O$ type, and spinel-like stuctures. The mixed oxides may exhibit strong basic properties as a function of the composition and thermal treatments, and give rise by reduction to well-dispersed and stable metal particles when reducible cations are present. In many hydrogenations, selectivity to the target compounds is enhanced by adding bases to the reaction medium, but few reports describe how the basic character of catalysts themselves may intervene. It would clearly be beneficial to replace these procedures by new catalyst formulations, in which the selectivity promotor belonged to the catalyst itself. This could be done by using intrinsically basic supports, which $M^{II}(M^{III})O$ mixed oxides could constitute.

We have thus shown previously that Ni/Mg/Al LDHs are excellent precursors of Ni/Mg(Al)O type catalysts for the hydrogenation of acetonitrile (3) and valeronitrile (4) into primary amines. The selectivity to ethylamine in the acetonitrile hydrogenation is maximum for materials with $Mg/(Mg + Ni) = 0.23$ and $(Ni + Mg)/Al \approx 3$ (3), calcined at 623 K and then reduced at 673 K (5). Calorimetric studies of ethylamine adsorption (3) and IR studies of adsorbed acetonitrile (5) provided evidence that surface acidity was the lowest in these materials. In the hydrogenation of nitriles, the condensed by-products are formed by transamination reactions between amines and imines, according to the formal reaction scheme shown in Fig. 1 (6). The selectivity between primary and higher amines is first determined by the nature of metal (7). However, on supported metal catalysts secondary reactions to higher amines can also proceed on acid sites of the carrier by condensation between amine and protonated imine to yield a protonated aminal. The *N*-alkylimine or enamine, formed after NH_3 and proton releases, is in turn hydrogenated on the metal sites to secondary or tertiary amine, respectively (bifunctional mechanism) (3, 8, 9). When the surface acidity

[1] To whom correspondence should be addressed.

0021-9517/00 $35.00

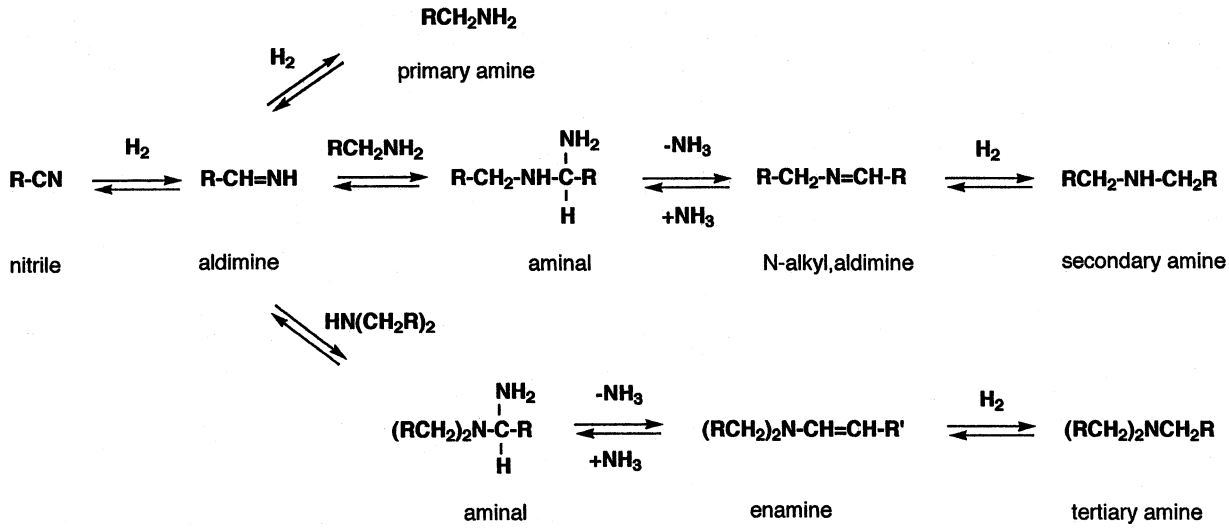

FIG. 1. Formal reaction scheme for nitrile hydrogenation.

decreases, by-product formation through this route is thus lowered.

Higher selectivities to primary amines could even be considered upon dedicated modifications of the metal phase. It is well known that the properties of metal catalysts can be fine-tuned by forming "bimetallic phases" (10). Higher selectivites to hexamethylenediamine in the hydrogenation of adiponitrile have thus been reached thanks to the promotion of Ni by Co, Cr, or Ti addition in Ziegler–Sloan–Laporte catalysts (11), and a patent claims for that reaction the use of catalysts prepared from LDHs of various compositions (12). Moreover, Co- and Ni-based catalysts are very selective for the hydrogenation of nitriles into primary amines (6, 7), and the synthesis of Co/Ni/Mg/Al mixed LDHs which leads to a wide variety of solids depending on the composition and the thermal treatments (13), has been reported recently. On that account, one might expect synergistic effects between Ni and Co when associated in the same catalyst prepared from Co/Ni/Mg/Al LDH. This work was thus aimed at the design of new catalytic materials prepared from Co/Ni/Mg/Al LDHs for the selective hydrogenation of nitriles into primary amines, with main focus on the modification of the metal phase; the gas-phase hydrogenation of acetonitrile was chosen as a model reaction.

EXPERIMENTAL

Preparation and Characterization of the Catalysts

Samples containing $Co^{2+}/Ni^{2+}/Mg^{2+}/Al^{3+}$ cations with a large range of compositions were prepared. They were obtained by coprecipitation at constant $pH = 9 \pm 0.2$ of an aqueous solution containing in appropriate amounts $Co(NO_3)_2 \cdot 6H_2O$, $Ni(NO_3)_2 \cdot 6H_2O$, $Mg(NO_3)_2 \cdot 6H_2O$, and $Al(NO_3)_3 \cdot 9H_2O$ with a solution of NaOH (1 M). The dropwise addition was performed at 293 K under vigorous magnetic stirring. The precipitated gels were heated in air at 353 K during 14 h, then centrifuged and washed several times with distilled water at 353 K. The solids were finally dried in an oven at 393 K for 72 h. Details are given elsewhere (13). All the solids exhibited the layered structure of LDHs as shown by XRD. The chemical analyses of the samples were carried out at the Service Central d'Analyse du CNRS (Solaize, France) by ICP-MS. Compositions of the samples are given in Table 1. The ratio $\Sigma M^{2+}/Al^{3+}$ was fixed at 3 in the starting synthesis solutions and ranged from 2.22 to 3 in the dried solids. We intended to prepare two families of samples, which can be identified by a near-constant Mg content ($Mg/(Mg + Ni + Co) \approx 0.25$–$0.29$) and variable $Ni/(Ni + Co)$ ratio on the one hand, and on the other hand by near-constant $Ni/(Ni + Co)$ ratio ($\approx$0.49–0.51) and variable Mg content.

The reducibility of Ni and Co species was examined by temperature-programmed reduction (TPR) after calcination of the solids in air at 393, 623, and 773 K. The experimental set-up was derived from that proposed classically (14). The detection was carried out with the thermal conductivity detector of a Shimadzu GC8 chromatograph. The experimental parameters were carefully selected to meet the recommendations of Monti and Baiker (15). An aliquot of the catalyst (50–100 mg) was activated first for 1 h in air at the temperature of calcination (ramp 10 K min^{-1}, flow = 100 cm^3 min^{-1}). The sample was then cooled to room temperature under He flow (purity > 99.995%). Helium was replaced by the reducing H_2/Ar gas (3/97, vol/vol, purity of both gases > 99.995%) and the linear temperature programme started from 293 to 1173 K (ramp 5 K min^{-1}, flow 20 cm^3 min^{-1}).

TABLE 1

Some Characteristics of the Co/Ni/Mg/Al LDHs

Sample	Chemical formula[a]	(Mg + Co + Ni)/Al	Mg/(Mg + Co + Ni)	Ni/(Co + Ni)	H/(Co + Ni)[b]
SR-19	$[Co_{0.53}Mg_{0.18}Al_{0.28}(OH)_2](CO_3^{2-})_{0.08}(NO_3^-)_{0.15} \cdot 0.64H_2O$	2.53	0.25	0	0.012
SR-21	$[Co_{0.41}Ni_{0.13}Mg_{0.19}Al_{0.27}(OH)_2](CO_3^{2-})_{0.05}(NO_3^-)_{0.23} \cdot 0.58H_2O$	2.60	0.26	0.24	0.042
SR-26	$[Co_{0.27}Ni_{0.26}Mg_{0.22}Al_{0.25}(OH)_2](CO_3^{2-})_{0.11}(NO_3^-)_{0.38} \cdot 0.46H_2O$	3.00	0.29	0.49	0.037
SR-22	$[Co_{0.14}Ni_{0.37}Mg_{0.21}Al_{0.27}(OH)_2](CO_3^{2-})_{0.07}(NO_3^-)_{0.19} \cdot 0.63H_2O$	2.63	0.29	0.73	0.09
SR-20	$[Ni_{0.53}Mg_{0.19}Al_{0.28}(OH)_2](CO_3^{2-})_{0.05}(NO_3^-)_{0.22} \cdot 0.62H_2O$	2.54	0.26	1	0.12
SR-23	$[Co_{0.36}Ni_{0.36}Al_{0.28}(OH)_2](CO_3^{2-})_{0.04}(NO_3^-)_{0.23} \cdot 0.50H_2O$	2.61	0	0.50	0.042
SR-24	$[Co_{0.32}Ni_{0.33}Mg_{0.09}Al_{0.26}(OH)_2](CO_3^{2-})_{0.12}(NO_3^-)_{0.22} \cdot 0.57H_2O$	2.86	0.12	0.51	0.048
SR-25	$[Co_{0.19}Ni_{0.19}Mg_{0.31}Al_{0.31}(OH)_2](CO_3^{2-})_{0.13}(NO_3^-)_{0.11} \cdot 0.75H_2O$	2.22	0.45	0.50	0.06

[a] After calcination at 393 K.
[b] After calcination at 393 K and reduction at 893 K.

The accessibility to Ni^0 and Co^0 phases was determined by H_2 chemisorption in a conventional static apparatus. The sample was reactivated at 773 K in H_2 overnight, then outgassed at the same temperature for 2 h at a pressure of 2×10^{-4} Pa. After saturation of the metal surface with H_2 at 373 K and 50–60 kPa, the desorption isotherm of H_2 was determined by step till 1 kPa. The H_2 uptake was estimated by the extrapolation to zero pressure of the linear part of the isotherm.

Acid–base properties of the carrier and metal function were characterized by adsorption of CD_3CN and CO, respectively, followed by FT-IR spectroscopy. The powdered precursors used for the IR experiments were those calcined at 393 K then reduced *ex situ* at 823 K. About 20 mg of the sample were pressed into a disk wafer of ca. 2 cm^2 surface. The *in situ* activation of the sample was performed in H_2 flow at 723 K for 15 h, then evacuation at the same temperature and a pressure of 2×10^{-4} Pa. Thereafter, the IR spectra were recorded at room temperature with a Nicolet 320 FTIR spectrometer at a resolution of 2 cm^{-1} (200 scans). A pressure of 530 Pa CO (>99.9%) was introduced into the IR cell, at full coverage, then evacuated at room temperature. The sample was outgassed by steps at increasing temperatures till low CO coverage. IR spectra were then collected at room temperature, after each evacuation. After the IR spectra of adsorbed CO were completed, the wafer was activated again *in situ* at 723 K in H_2. After evacuation at 723 K, the sample was cooled to room temperature and CD_3CN (Sigma, isotopic purity >99.9%) was admitted to the cell, at full coverage, then evacuated at room temperature. The IR spectra were then collected by following the same protocol as for the CO experiments.

Catalytic Test

The catalytic tests were performed in a microflow fixed-bed reactor operating at atmospheric pressure. The diameter of the reactor was about 8 mm, the catalyst bed was about 1.5 mm thick (grain size 0.063–0.125 mm). Prior to any measurements, 40 mg of catalyst were activated *in situ*. The sample was first calcined in an O_2/N_2 mixture (20/80, vol/vol) for 2 h at 393, 623, or 773 K (ramp 2 K min^{-1}), then cooled to room temperature under nitrogen. After that, the sample was reduced in a diluted hydrogen flow (H_2/N_2 10/90, vol/vol) at 723, 893, or 1023 K for 2 h (ramp: 2 K min^{-1}). Acetonitrile was fed by bubbling H_2 through a saturator at 273 K. The reaction mixture ($P(H_2) = 98$ kPa, $P(CH_3CN) = 3$ kPa) was then passed through the catalyst and the effluent was analyzed by sampling on line to a gas chromatograph (Perkin Elmer) equipped with a capillary column (30 m × 0.25 mm i.d., apolar phase) and a flame ionization detector. All connecting lines and commutation and sampling valves were placed in a hot box heated at 373 K in order to prevent any condensation. The following parameters were determined to evaluate the catalytic properties:

$$\text{acetonitrile conversion (mol\%)} = 100 \times (\text{acetonitrile}_{in} - \text{acetonitrile}_{out})/\text{acetonitrile}_{in}$$

$$\text{selectivity}_i\ \text{(mol\%)} = 100 \times (\text{corrected area})_i/(\text{sum of all corrected areas}).$$

The selectivities have been calculated from peak areas taking into account the different sensitivity factors in the flame ionization detector.

In the protocol for the catalyst tests, the sample was first passivated for 12 h at 393 K in the reaction medium ($P(H_2) = 98$ kPa, $P(CH_3CN) = 3$ kPa, flow = 30 cm^3 min^{-1}) to reach nearly steady-state conditions (3). The reaction temperature was then varied from 358 to 463 K, by alternating high and low values. In the course of the acetonitrile reaction with hydrogen, ethylamine (MEA) was the main organic compound formed, with selectivity normally higher than 70%. Diethylamine (DEA), *N*-ethyl,ethylimine (EEI), and triethylamine (TEA) usually appeared as by-products, and trace amounts (<1%) of ethane, methane,

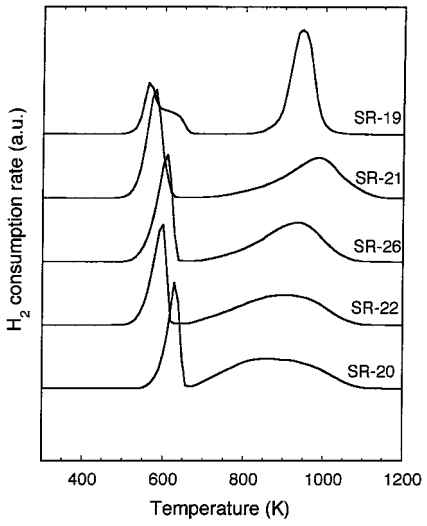

FIG. 2. Temperature-programmed reduction profiles of some Co/Ni/Mg/Al LDHs after calcination at 393 K; $m \approx 50$ mg, gas = H_2/Ar (3/97, vol/vol), ramp = 5 K min^{-1}, flow rate 20 cm^3 min^{-1}.

and oligomeric products were sometimes detected at high reaction temperatures.

RESULTS

Some typical TPR profiles of the Co- and Ni-containing samples, before and after calcination at 393, 623, and 773 K, are given in Figs. 2–4. The hydrogen uptakes are listed in Table 2. As general comments, one can observe:

(1) For all the samples two domains exist for H_2 consumption, in the low-temperature (<673 K, LT) and high-temperature (>673 K, HT) ranges. In some cases, these H_2 consumptions are featured by broad unresolved peaks with shoulders, which provide evidence of the reduction of several different species. The LT H_2 consumption peak is generally narrow, in contrast to the HT peak, which is narrow for the Ni-free sample but becomes broader and broader as the Ni content increases.

(2) There is a tendency to decrease of total H_2 consumption after calcination at high temperatures. This decrease, which can reach 40%, takes mainly place for the LT H_2 consumption.

(3) Two clear contributions exist in the LT H_2 consumption peak for the Ni-free sample (SR-19), which transform into a unique H_2 consumption peak for the Ni-containing samples (Fig. 2).

(4) An upward shift of the faster reduction rate for the HT peak occurs when the Mg content goes on at Ni/(Ni + Co) ratio constant (samples SR-23, -24, -26, and -25). However, this shift, which is by 50 K for samples calcined at 393 K (Fig. 3), becomes rather small after calcination at 773 K (≈30 K) (Fig. 4).

The accessibility to the metallic phase, H/(Co + Ni), was estimated from the H_2 chemisorption. The data are collected in Table 1 for the samples calcined at 393 K and

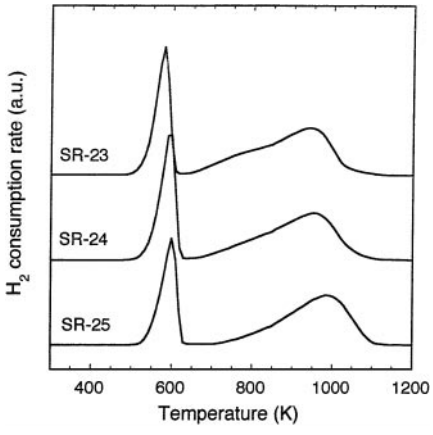

FIG. 3. Temperature-programmed reduction profiles of some Co/Ni/Mg/Al LDHs after calcination at 393 K; same conditions as in Fig. 2.

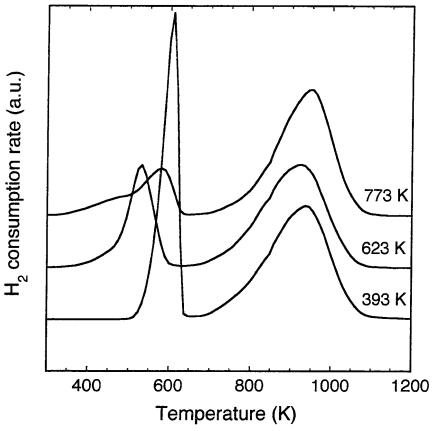

FIG. 4. Temperature-programmed reduction profiles of Co/Ni/Mg/Al LDH (SR-26) after calcination at various temperatures; same conditions as in Fig. 2.

TABLE 2

H_2/(Co + Ni) Molar Consumption Ratio in the LT (400–670 K) and HT (>670 K) Peaks of H_2 Consumption in the TPR Experiments on Co/Ni//Mg/Al Materials Calcined at Various Temperatures

	Calcined at 393 K			Calcined at 623 K			Calcined at 773 K		
Sample	LT	HT	Total	LT	HT	Total	LT	HT	Total
SR-19	0.38	0.89	1.27	0.42	0.81	1.23	0.33	0.78	1.11
SR-21	0.59	0.86	1.55	0.41	0.82	1.23	0.35	0.82	1.17
SR-26	0.59	0.88	1.57	0.33	0.80	1.13	0.22	0.84	1.06
SR-22	0.50	0.91	1.41	0.25	0.89	1.14	0.12	0.89	1.01
SR-20	0.48	0.95	1.43	0.15	0.92	1.07	0.04	0.93	0.97
SR-23	0.47	0.91	1.38	0.31	0.91	1.22	0.24	0.87	1.11
SR-24	0.50	0.90	1.40	0.38	0.92	1.20	0.23	0.78	1.01
SR-25	0.44	0.87	1.31	0.41	0.82	1.23	0.20	0.84	1.04

reduced at 893 K, which exhibited the most interesting catalytic behavior (*vide infra*). A clear tendency appears to increase metal accessibility upon the introduction of Ni. One can remark that good accessibilities to the metal phase were obtained in these materials in spite of the very high loading (50–60 wt% in metal). H/Co of ca. 0.03 was reported for an 8%Co/Al_2O_3 reduced at 673 K (16), and H/Ni of ca. 0.18 for a 21%Ni/MgO reduced at 673 K (17).

As was said above, the formation of by-products by condensation reactions between imines and amines can occur on both the metal and the support surfaces in the gas-phase hydrogenation of CH_3CN. On that account, the selectivity to these by-products may depend on (i) the electronic state and the topology of the metal phase and (ii) the acid–base properties of the support. The support and metal surfaces were thus probed by the adsorption of CD_3CN and CO, respectively, followed by FTIR spectroscopy.

Acetonitrile is a powerful probe which adsorbs on Brønsted and Lewis acid sites by the lone pair of the N atom and on basic sites through the methyl group as well (18). The IR spectra of the bare samples, recorded after H_2 activation at 893 K, show bands of extremely low intensities in the OH stretching region. After the adsorption of CD_3CN at room temperature, two groups of bands of medium intensities appear in the ranges 2400–2000 cm^{-1} (Fig. 5) and 1700–1100 cm^{-1} (Fig. 6).

The spectral region 2400–2000 cm^{-1} (Fig. 5) is mainly occupied by vibration modes of CD_3CN (18, 19), such as ν_{CN} and ν_{CD}. The latter appeared at ca. 2250 cm^{-1}, $\nu_{as}[CD_3]$, and 2110 cm^{-1}, $\nu_s[CD_3]$. The bands at ca. 2295 and 2170 cm^{-1} can be assigned to ν_{CN} of CD_3CN in electron-donor and electron-acceptor interactions, respectively (18). In this latter case, CD_3CN interacts indeed on a metal oxide according to the reaction

$$O^{2-}(\text{surf}) + CD_3CN \rightarrow OD^-(\text{surf}) + CD_2CN^-(\text{ads.}) \quad (1)$$

The broad band at 2295 cm^{-1} is due to the CN stretching frequency of CD_3CN in electron-donor interaction through the lone pair of N atom. In the case of Ni/Mg(Al)O catalysts from LDHs precursors (5), we proposed that this band can be convincingly attributed to CD_3CN adsorbed on very weak Mg^{2+} Lewis sites (20), and/or with Ni^0 sites (21).

It is worth noting that the adsorbed CD_2CN^- carbanion species exhibited higher thermal stability than CD_3CN in interaction with Mg^{2+} and/or Ni^0 sites. This is shown by the decrease of the relative intensities of the bands at 2295 and 2170 cm^{-1} upon evacuation at 323 K (Fig. 5).

Another group of bands appears in the region 1700–1100 cm^{-1} (Fig. 6) after adsorption of CD_3CN on NiCo/Mg(Al)O. They were assigned to acetamide-like compounds resulting from the reaction of acetonitrile on basic sites of oxides like Al_2O_3 (22), silica–magnesia (23), ZnO (24), or CeO_2 (25). The same bands were observed after adsorption of CD_3CN on Ni/Mg(Al)O (5). The nature of these acetamide species was not identified in more detail due to their complex structure.

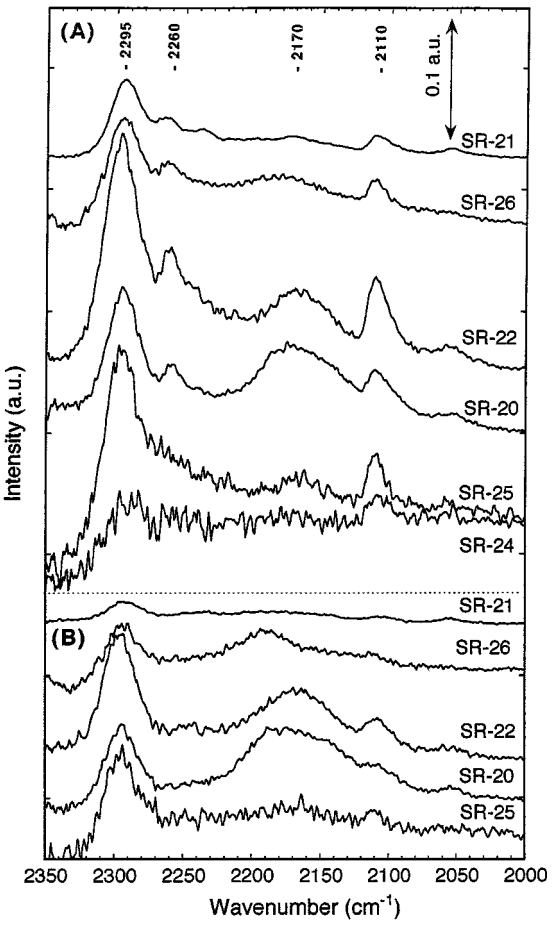

FIG. 5. IR spectra in the CN stretching domain of adsorbed CD_3CN on various Co/Ni/Mg/Al catalysts calcined at 393 K and reduced at 893 K; (A) after evacuation at room temperature, (B) after evacuation at 323 K.

Figure 7 shows the IR spectra of adsorbed CO in the region 2200–1700 cm^{-1}, characteristic of mono- and multicarbonyl species. It should be mentioned that bands of carbonate species, formed by interaction of CO with basic sites (18), appeared in the spectral region 1700–1200 cm^{-1}. The high-frequency band (HF, L band) between 2100 and 2000 cm^{-1} can be assigned to linear monocarbonyl species on metal sites. Ansorge and Förster (26, 27) reported a ν_{CO} at 2070 cm^{-1} for CO adsorbed on Co/Aerosil at full CO coverage, who shifted to slightly lower frequencies for CO on Co/MgO. On supported Ni catalysts, two bands of linearly adsorbed CO were observed at ca 2040 and 2070 cm^{-1} (28). The former was due to CO adsorbed on unperturbated Ni^0. The latter was assigned to CO bonded on Ni^0 atoms in close interaction with an oxide phase (unreduced Ni or other oxide phase). It should be mentioned that the presence of unreduced metal sites would give rise to two bands at 2195 cm^{-1} for CO on Ni^{2+} (28) and at ca. 2180 cm^{-1} for CO on Co^{2+} (26), never observed in our experiments.

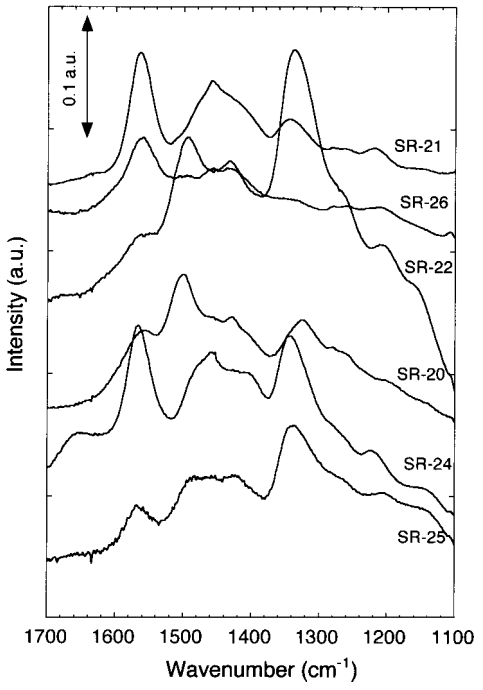

FIG. 6. IR spectra in the 1700–1100 cm^{-1} range of adsorbed CD_3CN, after evacuation at room temperature, on various Co/Ni/Mg/Al catalysts calcined at 393 K and reduced at 893 K.

The low-frequency bands between 2000 and 1800 cm^{-1} (LF, M bands) are generally assigned to multibonded CO species. These species rarely appear on supported Co catalysts (26, 29). In contrast, these species are commonly found on Ni-based catalysts (28, 30), with ν_{CO} at ca. 1935 cm^{-1} for Ni_2CO-bridged species and below 1900 cm^{-1} for Ni_xCO ($x = 3, 4$) multicentered species, at full CO coverage.

Tables 3–5 list the main catalytic properties of the samples in the hydrogenation of acetonitrile. The influence of the activation treatment on the reaction at 358 K is shown in Table 3 (the conversion was maintained at ca. 10% by tuning the contact time). Calcination at 393 K, then reduction at high temperature ($T \geq 893$ K), yields the most selective

TABLE 3

Main Catalytic Properties of the SR-26 Sample Calcined and Reduced at Various Temperatures, for the Reaction of Acetonitrile with Hydrogen at 358 K and Various Contact Times to Maintain the Conversion at ca. 10% ($P(H_2) = 98$ kPa, $P(CH_3CN) = 3$ kPa)

Temperature (K)		Rate × 10^6	Product selectivity (mol%)			
Calcination	Reduction	(mol g^{-1} s^{-1})	MEA	EEI	DEA	TEA
393	773	3.9	97.6	2.3	—	—
393	893	5.3	98.0	2.0	—	—
393	1023	5.2	98.0	2.0	—	—
573	773	4.1	95.0	3.7	1.3	—
573	893	6.4	97.5	1.8	0.5	—
773	893	6.8	97.0	1.9	1.1	—

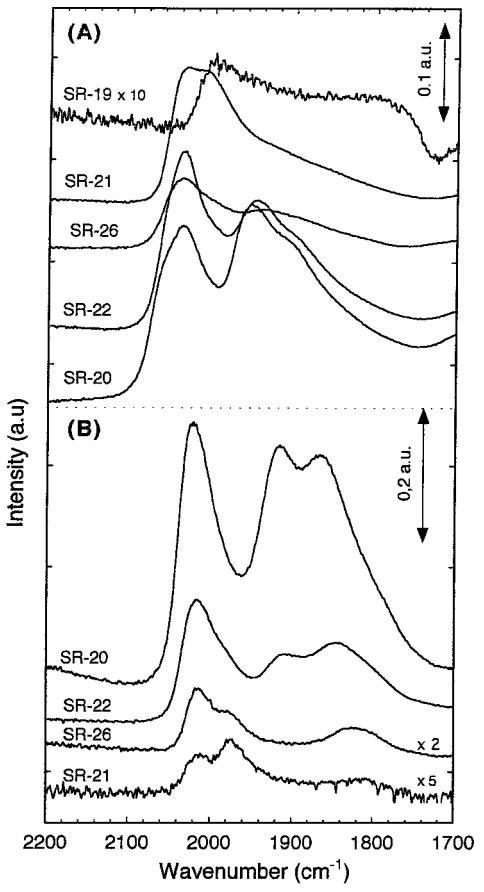

FIG. 7. IR spectra in the CO stretching domain of adsorbed CO on various Co/Ni/Mg/Al catalysts calcined at 393 K and reduced at 893 K; (A) after evacuation at room temperature, (B) after evacuation at 423 K.

catalysts to MEA. We have thus chosen to compare the samples with various Mg/(Mg + Co + Ni) and Ni/(Co + Ni) ratios activated by calcination at 393 K and reduction at 893 K. The catalytic data are reported in Tables 4 and 5

TABLE 4

Main Catalytic Properties of the Co/Ni/Mg/Al Catalysts, Calcined at 393 K and then Reduced at 893 K, for the Reaction of Acetonitrile with Hydrogen at 393 K ($P(H_2) = 98$ kPa, $P(CH_3CN) = 3$ kPa, flow 30 cm^3 min^{-1})

Sample	Rough molar composition Co/Ni/Mg/Al	Conv. (mol%)	Product selectivity (mol%)			
			MEA	EEI	DEA	TEA
SR-19[a]	1.9/0/0.7/1	4	67.2	31.2	0.6	—
SR-21	1.5/0.5/0.7/1	35	93.0	5.2	1.7	0.1
SR-26	1.1/1.1/0.9/1	90	94.6	0.2	5.0	
SR-22	0.5/1.4/0.8/1	93	95.2	0.1	4.3	0.3
SR-20	0/1.9/0.7/1	98	91.0	—	7.6	1.2
SR-23	1.3/1.3/0/1	90	92.0	0.2	7.3	0.4
SR-24	1.2/1.3/0.3/1	98.5	95.8	—	3.9	0.2
SR-25	0.6/0.6/1.0/1	99.9	95.3	—	4.2	0.4

[a] At 453 K.

TABLE 5

Main Catalytic Properties of the Co/Ni/Mg/Al Catalysts, Calcined at 393 K and then Reduced at 893 K, for the Reaction of Acetonitrile with Hydrogen at 358 K and Various Contact Times to Maintain the Conversion at ca. 10% ($P(H_2) = 98$ kPa, $P(CH_3CN) = 3$ kPa)

Sample	Rough molar composition Co/Ni/Mg/Al	Rate $\times 10^6$ (mol g^{-1} s^{-1})	TOF (h^{-1})	Product selectivity (mol%)			
				MEA	EEI	DEA	TEA
SR-21	1.5/0.5/0.7/1	3.3	59	95.5	3.3	1.2	—
SR-26	1.1/1.1/0.9/1	5.3	110	98.0	2.0	—	—
SR-22	0.5/1.4/0.8/1	5.9	52	95.8	1.5	2.5	0.1
SR-20	0/1.9/0.7/1	9.0	61	93.5	2.1	3.9	0.4
SR-23	1.3/1.3/0/1	2.9	41	91.5	3.5	4.7	0.3
SR-24	1.2/1.3/0.3/1	5.5	71	96.7	1.7	1.5	—
SR-25	0.6/0.6/1.0/1	4.1	66	96.2	1.7	1.9	—

for the reaction performed at 393 K and high conversion when possible, and at 358 K and low conversion (≈10%), respectively. One can remark that:

(1) The activity on Co/Mg(Al)O (SR-19) is very low, while it is much larger and of a similar order of magnitude for the other samples.

(2) Whatever the catalyst, the by-products are mainly EEI at low conversion, but DEA and TEA at high conversion.

(3) There is a synergistic effect between Ni and Co for the MEA selectivity with samples of constant ratio Mg/(Mg + Ni + Co), i.e., SR-21, SR-26, and SR-22.

DISCUSSION

During the TPR of monometallic Co/Mg/Al (31) and Ni/Mg/Al (32) composite materials, the first intense and narrow peak of H_2 consumption at ca. 550–600 K was due to the reduction of nitrate anions to NO mainly, as shown by coupling with mass spectrometry. Nitrates were decomposed for a great part in air at 623 K, and the decomposition was quasi-achieved after calcination at 773 K. The Co/Mg/Al samples exhibited a first reduction peak of Co in Co_3O_4 at 620 K ($Co_3O_4 \rightarrow CoO \rightarrow Co^0$) and a second reduction peak of Co in a mixed spinel phase $Co_xMg_{1-x}Al_2O_4$ from 970 to 1130 K, depending on the Mg content. On the other hand, the Ni/Mg/Al samples exhibited a broad peak of H_2 consumption from 650 to 1000 K due to the reduction of Ni in both Ni,Mg(Al)O mixed oxides and the $Ni_xMg_{1-x}Al_2O_4$ spinel phase (32). In these two series of Co- and Ni-based materials (31, 32) the temperature of faster reduction rates in the HT region (>650 K) was shifted upward when both the Mg content and the calcination temperature increased, due to higher interaction of Co and Ni in the respective mixed spinel phases.

In view of these observations we can conclude that the first intense and narrow peak of H_2 consumption, which steadily shifts from 550 to 620 K when moving from Ni-free to Co-free materials, is due to nitrate reduction (Figs. 2–4). The very large values of the ratio $H_2/(Co + Ni)$ (Table 2) in samples calcined at 393 K is perfectly in line with this statement. However, in this LT peak of H_2 consumption there is very likely a contribution from the reduction of Co_3O_4 and/or $Ni_xCo_{3-x}O_4$ species. This is very clear with the shoulder at 620 K for SR-19 calcined at 393 K (Fig. 2) and with the peak appearing at ca. 570 K for SR-26 calcined at 773 K (Fig. 4). Moreover, the $H_2/(Co + Ni)$ ratio is 1.10–1.20 for the samples with $Ni/(Co + Ni) \leq 0.5$ and calcined at 773 K (Table 2).

At quasi-constant Mg content and varying the Ni/(Co + Ni) ratio (samples SR-19, SR-21, SR-26, SR-22, and SR-20), there are clear changes of the HT reduction peak. It is narrower on the Co-rich samples, and it shifts to lower temperatures on the Ni rich samples. Moreover, these profiles for the Ni- and Co-containing samples appear as a single peak, and not the simple convolution of the reduction profiles of SR-19 and SR-20 samples. The temperature of faster reduction for SR-21 is even higher (≈1000 K) than that for SR-19 (≈900 K), showing thus a synergy between Ni and Co for a lower reducibility of the metal phase. This behavior is very likely due to the presence of a great proportion of Ni and Co in the same mixed-phase which could have a spinel-like or eventually a mixed-oxide-like structure.

On the Mg-free material (SR-23), two contributions exist in the HT peak at ca. 750 K (shoulder) and 950 K (Fig. 3), very likely assigned to the reduction of Ni(Al)O and $CoAl_2O_4$ species, respectively. The temperatures of faster reduction are indeed very similar to those found in the reduction of Ni/Al (32) and Co/Al (31) LDHs. When the Mg content increases the HT reduction peak becomes a unique and narrower contribution centered at ca. 970–990 K. This temperature is similar to that found with Ni/Mg/Al LDH at Ni/Mg = 1 (32) and is lower than that observed in the reduction of Co/Mg/Al at Co/Mg = 1 (31), which was 1100 K. On that account, we can reasonably propose that at least a part of Ni and Co are together in a spinel-like phase of a complex stoichiometry. A temperature of calcination up to 773 K has little effect on the reducibility of this phase (Fig. 4).

To sum up, the TPR experiments of Ni/Co/Mg/Al materials provide evidence of the reduction of two phases, Co_3O_4 and/or $Ni_xCo_{3-x}O_4$ in the LT region (570–620 K), and of several phases with probably a very complex quaternary spinel-like phase in the HT region (800–1000 K).

In the hydrogenation of CH_3CN over Ni/Mg(Al)O catalysts, we have previously reported that the selectivity to MEA was maximum for the sample with $Mg/(Mg + Ni) \approx 0.2$–0.25 (3). We have also demonstrated that the temperatures of calcination and reduction greatly influenced the

catalytic properties of Ni (5). We have therefore varied these conditions of activation for the sample SR-26. At the same conversion (≈10%, Table 3), the selectivity to MEA is high whatever the initial treatment of SR-26; however, a calcination at 393 K and reduction at 893–1023 K leads to the lowest formation of by-products. The degree of reduction after such an activation treatment was checked for SR-19 by TPR experiment on the activated sample, it was found of 90%. In the following all the samples were thus activated by calcination at 393 K and reduction at 893 K.

The first series of NiCo/Mg(Al)O catalysts we have studied was composed of samples with $Mg/(Mg + Co + Ni) \approx 0.25$ and $Ni/(Co + Ni)$ ratio from 0 to 1 (Tables 4, 5). The Co/Mg(Al)O sample (SR-19) was quasi-inactive, since the conversion was only 4% at 453 K. It was three orders of magnitude less active at 393 K than the Ni-containing catalysts, as extrapolated from the high-temperature data. However, the first addition of Ni (SR-21) immediatly boosts the activity in such a way that the TOF (Turn Over Frequency, or number of CH_3CN molecules converted per unit time and per Ni + Co surface atom) goes through a maximum for $Ni/(Co + Ni) = 0.5$ (Table 5). This provides evidence of a synergistic effect between Ni and Co which are in the same bimetallic aggregates very likely, as concluded also from TPR experiments.

Much more interesting is the evolution of selectivity in acetonitrile hydrogenation on NiCo/Mg(Al)O as a function of the $Ni/(Co + Ni)$. In a detailed previous study on Ni/Mg(Al)O (3), we reported that the total selectivity in condensed by-products (EEI, DEA, and TEA) was the highest at both high and low acetonitrile conversions. These condensed by-products are formed by the reactions between amines and imines, according to the formal reaction scheme shown in Fig. 1 (6). As mentioned above, on supported metal catalysts this condensation can proceed on the metal surface alone and/or the acid sites. This latter process allows us to understand why the selectivity to by-products decreased from low to medium conversions. This behavior seems in apparent contradiction to the formal consecutive reaction scheme shown in Fig. 1. Actually, part of the MEA formed at the reaction onset inhibits some acid sites of the support and therefore the bifunctionnally catalysed condensation reactions. There is thus a self-promotion of the catalyst by the MEA formation (3). For that reason, the differences in catalytic properties between the various samples will be more highlighted when comparing the MEA selectivity at similar and low conversion (≈10%, Table 5). In these conditions, it is worthy to note that the selectivity to MEA is the highest (≈98%) for $Mg/(Mg + Co + Ni) = 0.29$ (SR-26), which confirms the promoting effect of Mg for a quite similar amount as previously observed for Ni/Mg(Al)O catalysts (3). This could similarly be accounted for by a lower acidity of SR-26. Though weak, the IR signal of adsorbed CD_3CN evacuated at 323 K (Fig. 5B) shows that the relative intensity of the band at 2295 cm^{-1}, CD_3CN on Brønsted acid sites, is larger on SR-25 ($Mg/(Mg + Co + Ni) = 0.45$) compared to SR-26.

Moving from SR-21 to SR-26, SR-22, and SR-20 (Mg content quasi-constant), the selectivity to by-products EEI + DEA + TEA varies from 4.5% to 6.4%, going through a minimum value of 2% for NiCo/Mg(Al)O with $Ni/(Co + Ni) = 0.5$ (SR-26). On the other hand, the value found on Ni/Mg(Al)O (SR-20) is slightly lower than that we found previously on a similar catalyst, 93.5% compared to 93.9%, but at higher CH_3CN partial pressure (3). The synergistic effect between Ni and Co which decreases the formation of by-products can be accounted for by a modification of the NiCo metallic phase and/or the acid-base properties of the Mg(Al)O support. These two possibilities were evaluated after activation of the catalysts in H_2 by the adsorption of CO and CD_3CN followed by IR spectroscopy.

As said above CD_3CN probes the acid sites, band at 2295 cm^{-1}, and the basic sites, band at 2170 cm^{-1}. It was previously shown that a good correlation exists between the selectivity to EEI + DEA + TEA and the intensity ratio of the bands at 2295 and 2170 cm^{-1} for Ni/Mg(Al)O catalysts which suffered various activation treatments (5). The selectivity to EEI + DEA + TEA is 6.4, 4.1, and 2.0% at 10% CH_3CN conversion on samples SR-20, SR-22, and SR-26, respectively (Table 5). On the same samples and after evacuation at 323 K, the intensity ratio I_{2295}/I_{2170} is ca. 1.1, 2.1, and 1.5, respectively. There is thus no clear relationship between acido–basicity and selectivity to by-products. In contrast, it is clear that the lowest selectivity in by-products is reached in the presence of the bimetallic NiCo catalysts (SR-22, SR-26, SR-21, SR-24, and SR-25 samples, Table 5). On that account, it is tempting to ascribe the synergistic effect induced by the presence of both Ni and Co metal atoms to changes in the properties of the metallic function. In this respect, informations can be derived from the FTIR spectroscopy of adsorbed CO.

The main CO species on the NiCo/Mg(Al)O samples appear at ca 2035, 1935 and 1900 cm^{-1} (Fig. 7A and Table 6) at full CO coverage and can be assigned to NiCO, Ni_2CO and Ni_xCO species, respectively. However, a small contribution at ca 1980 cm^{-1} exists on the SR-26 and SR-21 samples after evacuation at 423 K, which can be assigned to CoCO, in agreement with the very small signal observed on SR-19. The various bands of CO species adsorbed on Ni are shifted to lower frequencies upon evacuation at increasing temperatures (Fig. 7B). This is due to the decrease of dipole–dipole coupling between neighboring adsorbed CO. Table 6 lists the ν_{CO} of the different species at full and low CO coverage for the samples with various $Ni/(Co + Ni)$ ratios. The relative abundance (in arbitrary unit) between the linear (L bands) and bridged or multicentered (M band) CO species has been estimated from the ratio of integrated optical

TABLE 6

Stretching Frequencies of CO Species Adsorbed in Different Configurations on the Metal Sites of Co/Ni/Mg/Al Catalysts

	ν_{CO} (cm^{-1})							
	Full CO coverage ($\theta \approx 1$)				Low CO coverage ($\theta < 0.1$)			
Sample	Ni–CO	Co–CO	$(Ni)_2CO$	$(Ni)_xCO$	Ni–CO	Co–CO	$(Ni)_2CO$	$(Ni)_xCO$
SR-20	2062s, 2038		1955	1905s	2008[a]			1810[a]
SR-22	2038		1950	1900s	2005[a]			1805[a]
SR-26	2038		1938		2012[b]	1977[b]		1830[b]
SR-21	2036	2010	1910s		2005[b]	1978[b]		1828[b]
SR-19		≈2000						

Note. s = shoulder.
[a] After desorption at 473 K.
[b] After desorption at 423 K.

density $A_L/(A_L + A_M)$ of the L and M bands. These values (Table 7), which are reported as a function of catalyst composition and evacuation temperature should only be considered as indicative due to the low resolution between L and M bands. Nevertheless, it is clear that this ratio increases upon the addition of Co. The decrease of bridged and multicentered CO species on Ni upon Co addition comes from a lower probability to encounter the required Ni_x sites to form the Ni_xCO complexes. This is a dilution effect of the Ni surface by Co, very similar to that reported in the case of NiCu bimetallics (33, 34).

On the other hand, CO becomes less strongly bonded upon Co addition. This is shown by the ratio of the integrated optical density $(A_L + A_M)_T/(A_L + A_M)_{293}$ after evacuation at increasing temperature T and at 293 K (Table 7). This ratio decreases more rapidly with temperature when the Co content increases.

To sum up, in the NiCo/Mg(Al)O catalysts, Ni and Co are together and in close interaction in the same bimetallic aggregates. This is in perfect agreement with the fact that Ni and Co melts crystallize to form a continuous series of solid solutions (35). The main effect of Co is the dilution of Ni surface into smaller ensembles which decreases the probability to form Ni_xCO complexes. CO desorbs more easily from these bimetallic aggregates than from monometallic Ni particles. These views of the metallic surface allow to develop an interpretation for the lowering in selectivity to condensed by-products, by considering in parallel the influence of Co addition on the main reaction.

The inelastic neutron scattering spectroscopy of CH_3CN on Raney Ni has shown that the adsorption is associative, that no C–H bond breaking occurs, and that the CN bond is parallel to the surface as an η_2 complex (36); the same was concluded for CH_3CN on evaporated Ni films (37) and on Pt(111) (38). In contrast, Friend *et al.* (39) proposed an η_1 complex bonded perpendicular to the Ni surface through the lone pair of N atom. From extended Hückel calculations, Bigot *et al.* (40) concluded that a possible competition between η_1 and η_2 forms occurred on Ni(111), but the η_2 form will prevail on Ni(100) and Ni(110) (41). It was also claimed that several Ni atoms would be involved in bonding the η_2 complex (36) and that the CN triple bond

TABLE 7

Integrated Optical Density (a.u.) of the IR L Bands (2100–2000 cm^{-1}) and M Bands (2000–1800 cm^{-1}) of CO on Co/Ni/Mg/Al Catalysts after Evacuation at Various Temperatures

	Sample					
	SR-20		SR-22		SR-26	
Temperature (K)	$A_L + A_M$	$A_L/(A_L + A_M)$	$A_L + A_M$	$A_L/(A_L + A_M)$	$A_L + A_M$	$A_L/(A_L + A_M)$
293	2400	0.37	1450	0.47	430	0.59
353	2400	0.36	1250	0.46	410	0.59
423	1600	0.34	580	0.43	100	0.67
473	180	0.13	10	0.23	—	—

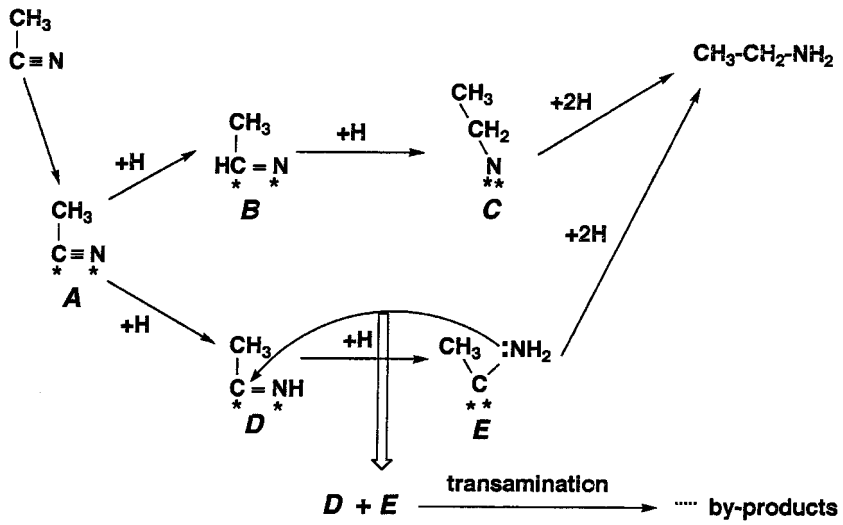

FIG. 8. Proposed elementary steps for the hydrogenation of acetonitrile on the Ni surface.

rehybridized to a double bond with both C and N atoms attached to the surface (36, 38).

On the other hand, the high-resolution electron-energy-loss spectroscopy of the thermal decomposition of MEA on Ni(111) has shown that the main adsorbed species is an aminomethylcarbene (**E** species, Fig. 8), which preferably might transform into an acimidoyl complex (**D** species, Fig. 8) at about 330 K (42). This last species is also the result of the first addition of an hydrogen atom to the activated adsorbed CH_3CN on Ni(111) (**A** species, Fig. 8) (43). The reaction scheme featured in Fig. 8 can thus be tentatively proposed for the hydrogenation of CH_3CN on the Ni phase. It should be pointed out that most of these species exchange bonds with several Ni atoms. In this respect, a decrease of TOF should occur upon substitution of Ni by Co atoms, since the latter are much less active. The reverse is actually true with the NiCo/Mg(Al)O catalysts and a slight increase of TOF happens for $Ni/(Co + Ni) = 0.5$ (SR-26, Table 5), in spite of the dilution by Co of the Ni surface shown by IR spectroscopy of CO. Two explanations can be put forward for this behavior:

(1) On the one hand, Co cannot activate CH_3CN at 353 K, but can do it for H_2, and Co atoms act as a reservoir for a pool of H atoms available for the hydrogenation reactions on neighboring Ni atoms. In this respect the dilution of Ni by Co is different from that by a really inactive metal such as Cu, which cannot act as a reservoir for H atoms at low temperature.

(2) On the other hand, an electronic modification of the Ni *d*-band may be considered, resulting in an enhanced reactivity of the adsorbed CH_3CN moities. This enhanced reactivity might originate from changes of heat of chemisorption and a more favorable position, from a kinetic point of view, on the volcano-shaped curve of Balandin for a reaction between two species in the adsorbed state. Proof of such a modification can be found in the easier desorption of CO from NiCo/Mg(Al)O compared to Ni/Mg(Al)O (Table 7).

If we consider now the transamination between imines and amines (Fig. 1), this reaction first proceeds from the nucleophilic addition of the primary amine (by the lone pair of the N atom) to the aldimino C atom to produce the aminal (6). This process, first described as occurring homogeneously in the liquid phase (44), can also take place in the adsorbed state on heterogeneous catalysts, and this is particularly true in gas phase reactions. It was even convincely demonstrated that this condensation should exclusively be catalyzed by the surface (45, 46). This condensation on the Ni surface between imines and amines can follow (i) an Eley–Rideal mechanism between adsorbed "imine" (species **D**, Fig. 8) and the amine occurring from the gas phase, or (ii) a Langmuir–Hinshelwood mechanism between two adsorbed species (species **D** and **E**, Fig. 8). In the former model, the size of the reaction site would not be very different from that of CH_3CN hydrogenation to MEA, and thus not very sensitive to the dilution of Ni surface by Co. In contrast, in the LH mechanism the size of the Ni ensemble required to accomodate both the "imine-" and "amine-like" adsorbed species is very likely larger. On that account, this reaction, leading to by-products EEI, DEA, and TEA, should be much more affected by alloying Ni with Co than the CH_3CN hydrogenation to MEA. This is indeed observed with NiCo/Mg(Al)O catalysts since the selectivity to EEI + DEA + TEA decreases whereas the TOF to CH_3CN hydrogenation increases upon the introduction of Co (Table 5).

The first step in the transamination reaction is the nucleophilic attack by the lone pair of N atom in amine to the C atom in imine. It comes out that in the adsorbed state, the LH mechanism of the transamination very likely involves the condensation between the **D** and **E** adsorbed species as the first step (Fig. 8). A very similar mechanism for the transamination on the metal surface was earlier proposed by Dallons *et al.* (45). The half-hydrogenated adsorbed nitrile (species **D**, Fig. 8) would react with vicinal NH_2-containing compounds to form a diamino species. The latter could rearrange through further hydrogenation and desorption steps into ammonia and secondary amine.

In this frame, the route through the nitrene **C** species would be more selective for MEA formation, in the CH_3CN hydrogenation, than the route through the aminomethylcarbene **E** species. From extended Hückel calculations the former was claimed to prevail on Ni(100) (41), whereas Ditlevsen *et al.* (43) privileged the latter route on Ni(111). It is very interesting to compare these aspects of the mechanism with very recent work from Huang and Sachtler (47) about acetonitrile deuteriation on NaY-supported metal catalysts. Ru/NaY is the most selective catalyst to ethylamine, in which the amine group contains predominantly H atoms, whereas the methylene group is almost CD_2. They conclude that the formation of ethylamine is not a simple addition of chemisorbed D atoms to the C≡N triple bond, but that a concerted reaction takes place with a H-donor molecule; the methyl group of the nitrile can act as H-donor. Huang and Sachtler (47) suggested that hydrogen transfer would take place on $CH_3CD_2N{=}Ru$ multibonded species, which are the intermediate **C** in Fig. 8. Ru, and Ni to a lesser extent, with high propensity to multiple bond formation exhibit high selectivity to primary amine. Very likely they promote the route through **B** and **C** intermediates on the metal surface.

CONCLUSIONS

Co/Ni/Mg/Al LDHs constitute good candidates as precursors of catalysts for the selective hydrogenation of nitriles into primary amines. Depending on the chemical composition and the calcination temperature, mixed-oxide and spinel-like phases of complex compositions are obtained. They lead to well-dispersed bimetallic phases of high metal loadings. The catalyst obtained from Co/Ni/Mg/Al (0.27/0.26/0.22/0.25) calcined at 393 K and reduced at 893 K exhibits the highest selectivity to ethylamine, 98.2% at 10% CH_3CN conversion. This is due to the lowering of the undesired consecutive transamination reaction which can occur between "imine-" and "amine-like" species on both the metal and acid sites, through a bifunctionnal mechanism, and on the metal sites alone.

The bifunctionnalized formation of condensed byproducts can be slightly attenuated by the tuned addition of Mg ($Mg/(Mg + Co + Ni) \approx 0.30$) which decreases the surface acidity.

Definite optimization of the hydrogenation Ni function, with respect to consecutive reactions, is achieved thanks to the formation of NiCo bimetallic phases. It is proposed that condensation reactions at the Ni sites occur through a Langmuir–Hinshelwood mechanism between two vicinal multibonded adsorbed species. The latter would be of the acimidoyl and aminomethylcarbene types. The introduction of Co into the catalyst dilutes the Ni phase in small ensembles less prone to accomodate neighboring multibonded species. The IR spectroscopy of adsorbed CO provided evidence of the dilution by Co of Ni surface in small ensembles.

ACKNOWLEDGMENTS

S.R. thanks the French Ministère de l'Education Nationale de la Recherche et de la Technologie for a scholarship.

REFERENCES

1. Cavani, F., Trifirò, F., and Vaccari, A., *Catal. Today* **11**, 173 (1991).
2. Trifirò, F., and Vaccari, A., *in* "Comprehensive Supramolecular Chemistry" (J. L Atwood, J. E. D. Davies, D. D. MacNicol, and F. Vögtle, Eds.), Vol. 7, p. 251. Pergamon, Oxford, 1996.
3. Medina Cabello, F., Tichit, D., Coq, B., Vaccari, A., and Dung, N. T., *J. Catal.* **167**, 142 (1997).
4. Tichit, D., Medina, F., Durand, R., Mateo, C., Coq, B., Suerias, J. E., and Salagre, P., *in* "Heterogeneous Catalysis and Fine Chemicals IV" (H.U. Blaser, A. Baiker, and R. Prins, Eds.), p. 297. Elsevier, Amsterdam, 1997.
5. Thi Dung, N., Tichit, D., Chiche, B. H., and Coq, B., *Appl. Catal. A General* **169**, 179 (1998).
6. de Bellefon, C., and Fouilloux, P., *Catal. Rev. Sci. Eng.* **36**, 459 (1994).
7. Volf, J., and Pasek, J., *in* "Catalytic Hydrogenation" (L. Cerveny, Ed.), p. 105. Elsevier, Amsterdam, 1986.
8. Freidlin, L. Kh., Sladkova, T. A., and Englina, F. F., *Kinet. Katal.* **3**, 417 (1962).
9. Verhaak, M. J. F. M., Van Dillen, A. J., and Geus, J. W., *Catal. Lett.* **26**, 37 (1994).
10. Ponec, V., and Bond, G. C., "Catalysis by Metals and Alloys." Elsevier, Amsterdam, 1995.
11. Balladur, V., Fouilloux, P., and de Bellefon, C., *Appl. Catal. A General* **133**, 367 (1995).
12. Cordier, G., and Popa, J. M., *French Patent* 2,738,757 (1995).
13. Ribet, S., Ph.D. Thesis. Montpellier, April 1999.
14. Lemaitre, J. L., *in* "Characterization of Heterogeneous Catalysts" (F. Delannay, Ed.), p. 34. Dekker, New York, 1984.
15. Monti, D. A. M., and Baiker, A., *J. Catal.* **83**, 323 (1983).
16. Kogelbauer, A., Goodwin, J. G., and Oukaci, R., *J. Catal.* **160**, 125 (1996).
17. Turlier, P., Praliaud, H., Moral, P., Martin, G. A., and Dalmon, J. A., *Appl. Catal.* **19**, 287 (1985).
18. Lavalley, J. C., *Catal. Today* **27**, 377 (1996).
19. Angell, C. L., and Howell, M. V., *J. Phys. Chem.* **73**, 2551 (1969).
20. Pelmenschikov, A. G., Morosi, G., Gamba, A., Coluccia, S., Martra, G., and Paukshtis, E. A., *J. Phys. Chem.* **100**, 5001 (1996).
21. Yim, S.-G., Son, D. H., and Kim, K., *J. Chem. Soc. Faraday Trans 1* **89**, 837 (1993).

22. Knözinger, H., Krietenbrink, H., Müller, H. D., and Schulz, W., *in* "6th International Congress on Catalysis" (G. C. Bond, P. B. Wells, and F. C. Tompkins, Eds.), p. 183. The Chemical Society, London, 1976.
23. Ritter, G., Noller, H., and Lercher, J. A., *J. Chem. Soc. Faraday Trans. 1* **78**, 2239 (1982).
24. Lavalley, J. C., and Gain, C., *C. R. Acad. Sci. Paris C* **288**, 177 (1979).
25. Binet, C., Jadi, A., and Lavalley, J. C., *J. Chim. Phys.* **89**, 31 (1992).
26. Ansorge, J., and Förster, H., *Z. Phys. Chem. N. F.* **118**, 113 (1979).
27. Ansorge, J., and Förster, H., *Z. Phys. Chem. N. F.* **95**, 255 (1975).
28. Primet, M., Dalmon, J. A., and Martin, G. A., *J. Catal.* **46**, 25 (1977).
29. Heal, M. J., Leisegang, E. C., and Torrington, R. G., *J. Catal.* **51**, 314 (1978).
30. Eischens, R. P., and Pliskin, W. A., *in* "Advances in Catalysis" (D. D. Eley, W. G. Frankenburg, V. I. Komarewsky, and P. B. Weisz, Eds.), Vol. 10, p. 1. Academic Press, San Diego, 1958.
31. Ribet, S., Tichit, D., Coq, B., Ducourant, B., and Morato, F., *J. Solid State Chem.* **142**, 382 (1999).
32. Tichit, D., Medina, F., Coq, B., and Dutartre, R., *Appl. Catal. A General* **159**, 241 (1997).
33. Soma-Noto, Y., and Sachtler, W. M. H., *J. Catal.* **34**, 162 (1974).
34. Dalmon, J. A., Primet, M., Martin, G. A., and Imelik, B., *Surface Sci.* **50**, 95 (1975).
35. Hansen, M., and Anderko, K., "Constitution of Binary Alloys," 2nd ed., p. 485. Genium Publishing Corporation, Schenectady, NY, 1991.
36. Hochard, F., Jobic, H., Clugnet, G., Renouprez, A., and Tomkinson, J., *Catal. Lett.* **21**, 381 (1993).
37. Kishi, K., and Ikeda, S., *Surface Sci.* **107**, 405 (1981).
38. Sexton, B. A., and Avery, N. R., *Surface Sci.* **129**, 21 (1983).
39. Friend, C. M., Muetterties, E. L., and Gland, J. L., *J. Phys. Chem.* **85**, 3256 (1981).
40. Bigot, B., Delbecq, F., and Peuch, V.-H., *Langmuir* **11**, 3828 (1995).
41. Bigot, B., Delbecq, F., Millet, A., and Peuch, V.-H., *J. Catal.* **159**, 383 (1996).
42. Gardin, D. E., and Somorjai, G. A., *J. Phys. Chem.* **96**, 9424 (1992).
43. Ditlevsen, P. D., Gardin, D. E., Van Hove, M. A., and Somorjai, G. A., *Langmuir* **9**, 1500 (1993).
44. von Braun, J., Blessing, G., and Zobel, F., *Chem. Ber.* **36**, 1988 (1923).
45. Dallons, J. L., Van Gysel, A., and Jannes, G., *in* "Catalysis of Organic Reactions" (W. E. Pascoe, Ed.), p. 93. Dekker, New York, 1992.
46. Huang, Y., and Sachtler, W. M. H., *Appl. Catal. A General* **182**, 365 (1999).
47. Huang, Y., and Sachtler, W. M. H., *J. Catal.* **184**, 247 (1999).